JACS
JOURNAL OF THE AMERICAN CHEMICAL SOCIETY
Article
pubs.acs.org/JACS

On the Bonding Nature of Ozone (O_3) and Its Sulfur-Substituted Analogues SO_2, OS_2, and S_3: Correlation between Their Biradical Character and Molecular Properties

Evangelos Miliordos and Sotiris S. Xantheas*

Physical Sciences Division, Pacific Northwest National Laboratory, 902 Battelle Boulevard, P.O. Box 999, MS K1-83, Richland, Washington 99352, United States

ABSTRACT: We investigate the bonding mechanism in ozone (O_3) and its sulfur-substituted analogues, SO_2, OS_2, and S_3. By analyzing their ground-state multireference configuration interaction wave functions, we demonstrate that the bonding in these systems can be represented as a mixture of a closed-shell structure with one and a half bonds between the central and terminal atoms and an open-shell structure with a single bond and two lone electrons on each terminal atom (biradical). The biradical character (β) further emerges as a simple measure of the relative contribution of those two classical Lewis structures emanating from the interpretation of the respective wave functions. Our analysis yields a biradical character of 3.5% for OSO, 4.4% for SSO, 11% for S_3, 18% for O_3, 26% for SOO, and 35% for SOS. The size/electronegativity of the end atoms relative to the central one is the prevalent factor for determining the magnitude of β: smaller and more electronegative central atoms better accommodate a pair of electrons facilitating the localization of the remaining two lone π-electrons on each of the end atoms, therefore increasing the weight of the second picture in the mixed bonding scenario (larger β). The proposed mixture of these two bonding scenarios allows for the definition of the bond order of the covalent bonds being $(3-\beta)/2$, and this accounts for the different O−O, S−S, or S−O bond lengths in the triatomic series. The biradical character was furthermore found to be a useful concept for explaining several structural and energetic trends in the series: larger values of β mark a smaller singlet−triplet splitting, closer bond lengths in the ground $^1A'$ and the first excited $^3A'$ states, and larger bond dissociation and atomization energies in the ground state. The latter explains the relative energy difference between the OSS/SOS and OOS/OSO isomers due to their different β values.

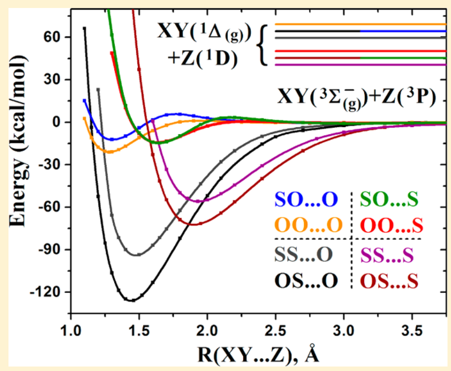

1. INTRODUCTION

The strong oxidant nature of ozone (O_3) has found a large number of applications in the industry of food preservation[1] or water disinfection processes.[2] Ozone can be harmful in the lower layer of atmosphere (troposphere) and is considered a greenhouse gas.[3] On the other hand, the ozone that is present in the stratosphere is beneficial for the terrestrial life protecting earth from the ultraviolet radiation.[4] In addition, ozone is an important reagent in chemistry mainly due to its ability to break double bonds via the process known as ozonolysis.[5]

The electronic structure of O_3 has been the Golden Apple of Discord (in Greek: *μῆλον τῆς ''Εριδος*) among theoretical chemists in the past. On the one end, based on generalized valence bond theory, Hay, Dunning, and Goddard suggested in 1975 that "the ground state of ozone is well represented as a biradical".[6] Under this premise, the electronic structure of O_3 is pictorially displayed[6] in Scheme 1.

Scheme 1. Biradical Structure of O_3

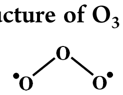

On the other end, Kalemos and Mavridis claimed in 2008 that the ground state of O_3 is a "genuine closed-shell singlet formed from O_2 ($^1\Delta_g$) and O (^{1}D)", suggesting[7] that its electronic structure rather corresponds to the two resonant structures shown in Scheme 2, which can be merged to the one shown in Scheme 3, by attributing one and a half bond to each O−O interaction.

Scheme 2. Closed-Shell Resonance Structures of O_3

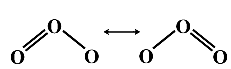

Scheme 3. Closed-Shell Structure of O_3

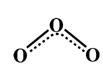

We have recently proposed an intermediate picture between those two opposing views with O_3 bearing a 19% biradical character.[8] Our proposition was based on the examination of the first two most important determinants of its multireference configuration interaction (MRCI) wave function at its complete active space self-consistent field (CASSCF) equilibrium

Received: October 21, 2013
Published: January 23, 2014

dx.doi.org/10.1021/ja410726u | J. Am. Chem. Soc. 2014, 136, 2808−2817

geometry. This suggestion was built upon earlier analyses[9] including ours,[10] however it was only recently rationalized (see Section 2 of the paper in conjunction with ref 8). Our recent formulation was furthermore able to correctly describe the trends in the observed singlet−triplet splitting for the OXO (X = F^+, O, NH, CH_2) molecular species as well as their energy barrier to the ring conformation from their biradical character (β), viz. a larger β brings the singlet and triplet states closer together and decreases the energy barrier.[8]

In an attempt to shed more light on the bonding mechanism of O_3 and relate its electronic structure to the corresponding electronic states of its constituent fragments, we have constructed the potential energy curves (PECs) describing the O_2 + O interaction[11] and monitored the variation of the total wave function as the O_2 and O fragments approach each other. The same strategy was followed for ozone's sulfur-substituted analogues, viz. OSO, SOO, SOS, SSO, and S_3, in an attempt to investigate the correlation between the molecular properties and the biradical character of a molecular system. In this paper we report the equilibrium structures and relative energetics of the first four electronic states of all species that correlate to the ground-state fragments, viz. O_2 ($X\,^3\Sigma_g^-$), S_2 ($X\,^3\Sigma_g^-$), SO ($X\,^3\Sigma^-$), O (^3P), and S (^3P). The ensuing analysis accounts for the different O−O, S−S, or S−O bond lengths in the aforementioned species as well as provides an explanation for the stabilization of the SSO and OSO species over their SOS and SOO isomers, respectively. The organization of the paper is as follows: In Section 2 we outline the methodology we adopted for choosing a flexible wave function that allows us to define the biradical character of a molecular system. In Section 3 we describe the electronic structure of the first four states of the examined systems in more detail, initially focusing on O_3 and subsequently expanding the results and discussion on its sulfur analogues. In Section 4 we discuss the correlation between the biradical character of the triatomic systems and corresponding molecular properties of their constituent fragments such as the location of their dissociation and excited-state asymptotes. We further use these rules to explain the correlation between β and the bond dissociation energies, corresponding geometries, and relative energetics. Our conclusions are finally presented in Section 5.

2. METHODOLOGY

The complete active space self-consistent field (CASSCF) approach was employed to build the reference wave function for all systems studied in this paper. The active space consists of all valence orbitals and electrons, i.e. 2s2p for oxygen and 3s3p for sulfur. Therefore in all cases the CASSCF wave function was constructed by allowing 18 active electrons to occupy 12 orbitals. We subsequently allowed all possible single and double excitations out of all those active valence orbitals to the virtual space, and the resulted configurations were variationally coupled according to the MRCI scheme. To keep the number of configurations tractable, we applied the internal contraction scheme (icMRCI) of Werner and co-workers,[12] as implemented in the MOLPRO suite of codes.[13] The correlation consistent basis sets of triple-ζ quality augmented with a set of diffuse functions (aug-cc-pVTZ) of Dunning and co-workers[14] were used. For sulfur, the basis set was also supplied with an additional d function (aug-cc-pV(T+d)Z) that was introduced in order to mend the convergence toward the complete basis set limit.[15]

At each point on the four lowest ($\tilde{X}^1A'$, $^3A''$, $^3A'$, $^1A''$) XY−Z PECs (X, Y, and Z being either O or S), that will be discussed in the subsequent sections, the XY−Z distance was varied, while the XY bond length and the X−Y−Z angle were optimized for each XY−Z distance at the icMRCI level of theory. However, the geometries for the second and third states of $^1A'$ symmetry ($2^1A'$ and $3^1A'$) were kept fixed to those of the ground state, $\tilde{X}^1A'$. Finally, all quintet states are found to be repulsive and their XY bond length was kept fixed to the equilibrium value of the corresponding free XY molecule. The C_{2v} optimum geometries for all four species (O_3, OSO, SOS, S_3) for all first four states were confirmed to be minima on the corresponding potential energy surfaces, as indicated by the fact that the energy increases along the single symmetry-breaking asymmetric stretching mode leading to C_s symmetry. The only exception is the lowest $^1A''$ state of O_3 with an imaginary harmonic frequency of 106 cm^{-1}. All calculations were performed under C_s symmetry, which is the lowest possible symmetry for the triatomic molecules.

The ground-state wave function at the (XYZ) equilibrium geometries has the form:

$$|\tilde{X}\,^1A'\rangle = (c_1|\pi_0^2\pi_1^2\rangle - c_2|\pi_0^2\pi_2^2\rangle)/\sqrt{c_1^2 + c_2^2} \tag{1}$$

where $\pi_k^2 \equiv \pi_k\overline{\pi}_k$ and $\pi_k(\overline{\pi}_k)$ is used to denote spin "up"("down"), $\uparrow(\downarrow)$.[16] For the case of O_3, c_1 = 0.872, c_2 = 0.274 (ref 8) and π_0, π_1, π_2 are the three out-of-plane valence molecular orbitals (π_0 = 1a″, π_1 = 2a″, π_2 = 3a″).[10] In eq 1 the orbitals lying on the molecular plane were not included, while components with coefficients smaller than 0.1 were ignored. Eq 1 can be rewritten as

$$|\tilde{X}\,^1A'\rangle = \frac{c_1 - c_2}{\sqrt{c_1^2 + c_2^2}}|\pi_0\overline{\pi}_0\pi_1\overline{\pi}_1\rangle + \frac{\sqrt{2}\,c_2}{\sqrt{c_1^2 + c_2^2}}\frac{|\pi_0\overline{\pi}_0\pi_1\overline{\pi}_1\rangle - |\pi_0\overline{\pi}_0\pi_2\overline{\pi}_2\rangle}{\sqrt{2}} \tag{2}$$

After transforming the π_1 and π_2 molecular orbitals according to ref 8, $\pi_\pm = 2^{-1/2}(\pi_1 \pm \pi_2)$, eq 2 can be recast in the form:

$$|\tilde{X}\,^1A'\rangle = \frac{c_1 - c_2}{\sqrt{c_1^2 + c_2^2}}|\pi_0\overline{\pi}_0\pi_1\overline{\pi}_1\rangle + \frac{\sqrt{2}\,c_2}{\sqrt{c_1^2 + c_2^2}}\frac{|\pi_0\overline{\pi}_0\pi_+\overline{\pi}_-\rangle - |\pi_0\overline{\pi}_0\overline{\pi}_+\pi_-\rangle}{\sqrt{2}} \tag{3}$$

The first term of the wave function described by eq 3 is a closed-shell determinant, while the second term represents an open-shell two-electron normalized wave function with spin quantum number $S = M_S = 0$. Moreover, the π_1 and π_2 orbitals can be denoted as[10] [+ 0 −]

Table 1. Coefficients of the Two Most Important Electronic Configurations of the icMRCI Wavefunction (c_1, c_2), Biradical Character (β) of the $\tilde{X}^1A'$ State from eq 4, Atomization Energies (AE, kcal/mol) and Binding Energies (D_e, kcal/mol) with Respect to the Ground-State Fragments, $O_2(^3\Sigma_g^-)$, $SO(^3\Sigma^-)$, $S_2(^3\Sigma_g^-)$, $O(^3P)$, and $S(^3P)$ for the O_3, SO_2, OS_2, and S_3 Molecules[a]

(X−Y−Z) molecule	c_1	c_2	β	D_e (X−YZ) (kcal/mol)	D_e (XY−Z) (kcal/mol)	AE[b] (kcal/mol)
O−O−O	0.872	−0.274	0.180	22.0 (26.105 ± 0.392)[c]	22.0 (26.105 ± 0.392)[c]	135.9
O−S−O	0.910	−0.122	0.035	126.5	126.5 (130.735)[d]	242.7
O−O−S	0.848	−0.328	0.260	11.6	14.3	127.6
S−O−S	0.826	−0.382	0.353	14.4	14.4	130.1
O−S−S	0.899	−0.135	0.044	94.2	73.1 (≤91)[e]	188.6
S−S−S	0.869	−0.208	0.108	55.7	55.7	149.9

[a]Experimental binding energies are shown in parentheses. [b]With respect to O(^3P) and S(^3P). [c]Ref 27. [d]Ref 23a. [e]Ref 28.

and [− + −], the signs indicating the orientation of the atomic p_π orbitals of the three atoms in a direction perpendicular to the molecular plane, and hence the π_+, π_- orbitals are approximately [0 + −] and [+ − 0], thus exhibiting a larger localization on the end atoms. The square of the coefficient of the second term in eq 3 can be assigned as the biradical character β, viz.

$$\beta = \frac{2c_2^2}{c_1^2 + c_2^2} \tag{4}$$

Note that the above definition of β encompasses the correct limits for the two extreme cases, i.e., $\beta = 0$ (no biradical character) when $c_2 = 0$ (only the first term of eq 3 corresponding to a closed-shell configuration survives) and $\beta = 1$ (perfect biradical) when $c_1 = c_2$ (only the second term of eq 3 corresponding to an open-shell two-electron configuration survives). We note that in the present study the c_1 and c_2 coefficients are obtained from icMRCI calculations at the icMRCI optimum geometries (icMRCI//icMRCI), while in ref 8 they were reported from icMRCI//CASSCF calculations. For this reason the values we reported previously[8] are slightly different than the current ones, which are listed in Table 1, along with the corresponding biradical character of the species. It should be emphasized that eqs 2 and 3 are provided for purely pedagogical purposes in order to render justification for the definition of β as the square of the coefficient of the second term (open-shell two-electron wave function) in eq 3, and the ensuing analysis is performed directly from eq 1, viz. no tranformation to the $\pi_\pm$ orbitals is necessary.

3. BONDING STRUCTURE OF O_3 AND ITS SULFUR ANALOGUES

3.1. Ozone. We begin our discussion of the bonding in the titled molecules with the case of ozone. The ground states of O_2 and O are $X^3\Sigma_g^-$ and ^3P, respectively. Their first two excited states are $^1\Delta_g$, $^1\Sigma_g^+$ (for O_2) and ^1D, ^1S (for O), experimentally lying 7918.1, 13195.1 and 15789.9, 33714.6 cm^{-1} (M_J averaged) above the respective ground states.[17] As a result, the lowest adiabatic channel leading to the formation of O_3 from these two fragments is O_2 ($X\,^3\Sigma_g^-$) + O (^3P), followed by O_2 ($^1\Delta_g$) + O (^3P), O_2 ($^1\Sigma_g^+$) + O (^3P), and O_2 ($^1\Delta_g$) + O (^1D). Under C_s symmetry, the first channel gives rise to two states of $^{1,3,5}A'$ symmetry and one of $^{1,3,5}A''$ symmetry, while the second and third ones result in triplet states only. The fourth channel produces five $^1A'$ and five $^1A''$ states. Peyerimhof and co-workers[18] have studied the PECs of several states, while Schinke and co-workers have devoted a large number of theoretical studies in examining the spectroscopic characteristics of O_3.[19] Detailed accounts of the electronic states of O_3 can be found in refs 7, 11, 19, and 20. In this study we focus on all states arising from the O_2 ($X\,^3\Sigma_g^-$) + O (^3P) asymptote and the one $^1A'$ state from the O_2 ($^1\Delta_g$) + O (^1D) asymptote aiming at elucidating the electronic structure of O_3 and explaining the shape of the corresponding PECs, which are shown in Figure 1.

As mentioned earlier, there are three quintet states stemming from the ground-state fragments. In those states all lone electrons of O_2 and O remain "uncoupled", thus avoiding the formation of a covalent bond. Besides, all valence orbitals of O_2 and O are either singly or doubly occupied, ruling out the possibility of a dative bond. Consequently, all quintet states are repulsive (see Figure 1). On the other hand, the triplet and singlet states facilitate the formation of one covalent bond, according to the diagrams shown in Schemes 4 and 5.

For the sake of clarity, only the 2p orbitals are depicted in Schemes 4 and 5. The 2s orbitals are, of course, mixed with all six 2p orbitals on the O_3 plane (a′ irreducible representation) allowing any angle between the two O−O bonds. Besides the "open" global minimum at an O−O−O angle ϕ = 116.7° (cf. Table 2), there exists a local "ring" minimum at ϕ = 60° and

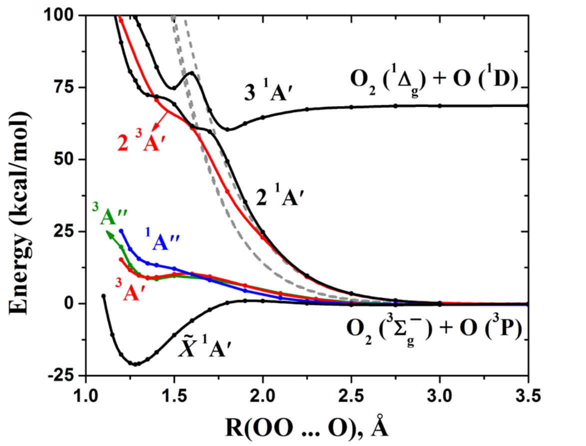

Figure 1. Potential energy curves (PECs) of O_3 as a function of the OO···O distance. The repulsive curves indicated by the dashed lines correspond to the quintet states.

Scheme 4. Covalent Bonding for the Lowest $^{1,3}A'$ States of O_3

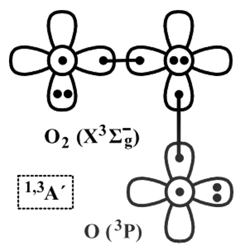

Scheme 5. Covalent Bonding for the Lowest $^{1,3}A''$ States of O_3

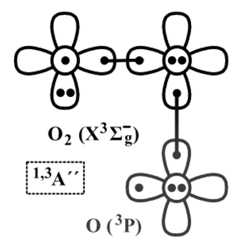

a conical intersection with the lowest excited state of the same symmetry, which has been previously investigated in detail by Ruedenberg and co-workers.[11,21] Finally, there exists one more bonding scenario involving the third possible O(^3P) component, which results in a dissociative (nonbonding) interaction shown in Scheme 6.

In agreement with the bonding scenarios illustrated in Schemes 4−6, there exists one $^1A''$ and one $^3A''$ purely repulsive PECs in Figure 1. Surprisingly, among the other four states only the $\tilde{X}^1$ A′ state is strongly bound producing the global minimum with a binding energy of 22.0 kcal/mol (at the corresponding level of theory used in this study). The rest three states have a repulsive nature at long distances, forming a shallow well around $r(O_2{-}O)$ = 1.35 Å, but with energy still higher than the lowest energy fragments. All three states lie close to each other and are at least 30 kcal/mol higher than the ground state. Their repulsive nature can be attributed to the fact that the actual picture of the X $^3\Sigma_g^-$ state of O_2, shown in Scheme 7, bears one and a half electrons in each p_π orbital. Hence, the orbital of O_2 participating in the bonding scenario shown in Schemes 4 and 5 occupies 1.5 (instead of one) electrons, thus hindering a direct bond formation. It seems, however, that at shorter distances

Table 2. icMRCI/[O: aug-cc-pVTZ, S: aug-cc-pV(T+d)Z] Geometries (r_1, r_2, φ) and Total (E) and Excitation (T_e) Energies of the First Four Electronic States of O_3, SO_2, OS_2, and S_3 Correlating Adiabatically to the Ground-State Fragments[a]

state C_s/C_{2v}	r_1 (Å)	r_2 (Å)	φ (°)	E (au)	T_e (kcal/mol)
			O–O–O		
$^1A'/^1A_1$	1.279 (1.2728)[b]	1.279 (1.2728)[b]	116.7 (116.754)[b]	−225.09680720	0.0
$^3A''/^3A_2$	1.348 (1.345)[c]	1.348 (1.345)[c]	98.7 (98.9)[c]	−225.04902500	30.0 (28.5)[d]
$^3A'/^3B_2$	1.361	1.361	108.5	−225.04777075	30.8 (30.0)[e]
$^1A''/^1A_2$	1.353	1.353	99.4	−225.04073250	35.2 (∼36.9)[e]
			O–S–O		
$^1A'/^1A_1$	1.438 (1.4308)[f]	1.438 (1.4308)[f]	119.4 (119.2)[f]	−547.93663495	0.0
$^3A''/^3A_2$	1.542	1.542	94.5	−547.81209413	78.2
$^3A'/^3B_2$	1.564	1.564	105.4	−547.80719029	81.2
$^1A''/^1A_2$	1.543	1.543	94.7	−547.80393742	83.3
			S–O–O		
$^1A'$	1.639	1.308	119.4	−547.75349357	0.0
$^3A''$	1.669	1.362	100.7	−547.72882067	15.5
$^3A'$	1.693	1.359	111.5	−547.72621436	17.1
$^1A''$	1.685	1.355	102.3	−547.72311585	19.1
			S–O–S		
$^1A'/^1A_1$	1.640	1.640	124.3	−870.42786790	0.0
$^3A''/^3A_2$	1.668	1.668	105.4	−870.41564324	7.7
$^3A'/^3B_2$	1.672	1.672	116.6	−870.41262407	9.6
$^1A''/^1A_2$	1.669	1.669	107.5	−870.41193147	10.0
			S–S–O		
$^1A'$	1.897 (1.8842)[g]	1.475 (1.4562)[g]	118.0 (117.9)[g]	−870.52136691	0.0
$^3A''$	2.092	1.494	105.9	−870.45557239	41.3 (∼40)[h]
$^3A'$	2.102	1.507	108.1	−870.45098159	44.2
$^1A''$	2.117	1.491	105.1	−870.45107309	44.1
			S–S–S		
$^1A'/^1A_1$	1.934 (1.914)[i]	1.934 (1.914)[i]	117.6 (117.3)[i]	−1193.13107581	0.0
$^3A''/^3A_2$	2.005	2.005	94.5	−1193.09330763	23.7
$^3A'/^3B_2$	2.028	2.028	107.8	−1193.08818227	26.9
$^1A''/^1A_2$	2.010	2.010	95.0	−1193.08730341	27.5

[a]Experimental values are shown in parentheses. Distances correspond to the ones between the first and the second (r_1) and between the second and the third atoms (r_2), respectively. [b]Ref 29. [c]Ref 30. [d]Ref 31. [e]Ref 32. [f]Ref 33. [g]Ref 34. [h]Ref 35. [i]Ref 23].

Scheme 6. Nonbonding Interaction for the First Excited $^{1,3}A''$ States of O_3

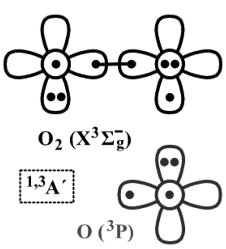

Scheme 7. Electronic Structure of the X $^3\Sigma_g^-$ Ground State of O_2

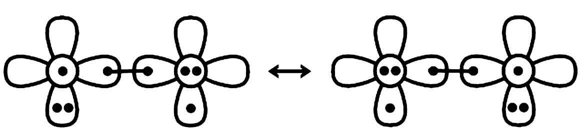

along the PEC the binding interaction illustrated in Schemes 4 and 5 is eventually initiated.

The icMRCI wave function at the equilibrium geometry of the first four electronic states of O_3 under C_s symmetry (accounting only for the valence orbitals and omitting the 1a′ through 6a′ doubly occupied valence orbitals and using bars to indicate orbitals with spin "down") are:

$$|\tilde{X}\,^1A'\rangle \approx 0.87|7a'^2 1a''^2 2a''^2\rangle - 0.27|7a'^2 1a''^2 3a''^2\rangle \qquad (5)$$

$$|^3A'\rangle \approx 0.92|7a'^2 1a''^2 2a'' 3a''\rangle \qquad (6)$$

$$|^3A''\rangle \approx 0.89|7a' 1a''^2 2a''^2 3a''\rangle \qquad (7)$$

$$|^1A''\rangle \approx 0.87|1a''^2 2a''^2 (7a'\overline{3a''} - \overline{7a'}3a'')\rangle \qquad (8)$$

The last three states are consistent with the proposed Schemes 4 and 5, with the $^1A''$ state being the open-singlet partner of the $^3A''$ state. However, the $\tilde{X}^1$ A′ state does not resemble the $^3A'$ state (recall that these have very different energies). To further analyze this behavior, we monitor the change of the ground-state wave function with respect to the O_2–O distance. At infinity, we have (now omitting the $1a''^2$ as well):

$$\begin{aligned}|\tilde{X}\,^1A'\rangle_\infty = {}& 0.56|\overline{7a'}11a'\overline{2a''}3a''\rangle + 0.56|7a'\overline{11a'}2a''\overline{3a''}\rangle \\ & - 0.28|\overline{7a'8a'}2a''3a''\rangle - 0.28|7a'8a'\overline{2a''3a''}\rangle \\ & - 0.28|7a'\overline{8a'2a''}3a''\rangle - 0.28|\overline{7a'}8a'2a''\overline{3a''}\rangle)\end{aligned} \qquad (9)$$

At a distance of 3.5 Å, four additional terms emerge that can be summarized as $0.07|(7a'^2 - 8a'^2)(2a''^2 - 3a''^2)\rangle$ and are

dx.doi.org/10.1021/ja410726u | J. Am. Chem. Soc. 2014, 136, 2808–2817

combined with the first two determinants of eq 9 with a coefficient of 0.40. These new (four) terms signal the "interaction" of the ground-state PEC with an excited state, viz. the third $^1A'$ state stemming from the $O_2(^1\Delta_g)$ + $O(^1D)$ asymptote. Two of these new terms are becoming gradually more important (i.e., their coefficients are increasing), and they eventually become the dominant configurations at the equilibrium geometry.

The previous analysis supports the position that the ground state of O_3 does indeed originate from the excited-state fragments $O_2(^1\Delta_g)$ + $O(^1D)$ as first proposed by Kalemos and Mavridis.[7] These authors reached the same conclusion by correlating the $^1\Delta_g$ state of linear O_3 with the $O_2(^1\Delta_g)$ + $O(^1D)$ channel and observing the smooth transition from the $^1\Delta_g$ to the ground state of the bent O_3 molecule. In addition, they referred to O_3 as a "genuine closed-shell singlet" with its bonding scenario depicted by Scheme 2. Recall, however, that the form of the $\tilde{X}^1A'$ state does allow for the assignment of biradical character that can be visualized by the bonding diagrams in Schemes 1 or 4. Therefore, our proposed picture describing the electronic structure of the ground state of O_3, shown in Scheme 8, is that of a 82% to 18% mixture of the two extreme bonding diagrams shown in Schemes 1 and 3.

Scheme 8. Proposed Bonding Diagram for O_3

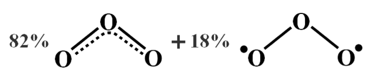

Note that our current value for the biradical character of O_3 (18%) is different than the one previously reported (44%) in ref 10, since the latter used the square root of the present expression, eq 4. Justification for the present definition of β, introduced previously by us in ref 8, is provided from eq 3, and it is consistent with the quantum mechanical association of probability with the square of the corresponding coefficient.

The equilibrium geometries and excitation energies for the first four electronic states of the various triatomic molecules in this study are listed in Table 2. Observe that the geometries of the $^{1,3}A''$ states are very similar. On the contrary, the O−O distance of the $\tilde{X}^1$ A′ state (1.279 Å) is much shorter than that of the $^3A'$ (1.361 Å) and the $^{1,3}A''$ (∼1.35 Å) states. The reason is because of the single bond that is present in the last three states, while the O−O bond order in the $\tilde{X}^1$ A′ state can be estimated, according to Scheme 8, as 0.82 × 1.5 + 0.18 × 1.0 = 1.41.

3.2. Ozone's Sulfur Analogues: SO_2, OS_2, and S_3. We now turn our discussion to the bonding patterns of ozone's sulfur analogues, i.e., triatomic molecules that result from O_3 when replacing one or more oxygen atoms with sulfur. Their equilibrium geometries and excitation energies for the first four electronic states are listed in Table 2. The PECs of the SO_2 (OSO, OOS) and OS_2 (SOS, OSS) isomers are shown in Figures 2−5. For the asymmetric OOS and OSS isomers, both possibilities, viz. O···OS, OO···S (Figure 3a,b) and OS···S, O···SS (Figure 5a,b) are included. The PECs of S_3, previously reported by Peterson et al.,[22] are shown at the same level of theory in Figure 6 for completeness and comparison with the other homologous triatomic molecules in this study.

More detailed studies on the structures and spectra of the above molecules can be found in the literature.[22,23] The largest biradical character is that of SOS (β = 0.353), whereas the smallest one (almost 10 times smaller) is for OSO (β = 0.035). The ozone molecule is located almost in the middle of those values (β = 0.180). In our earlier study[8] we examined the

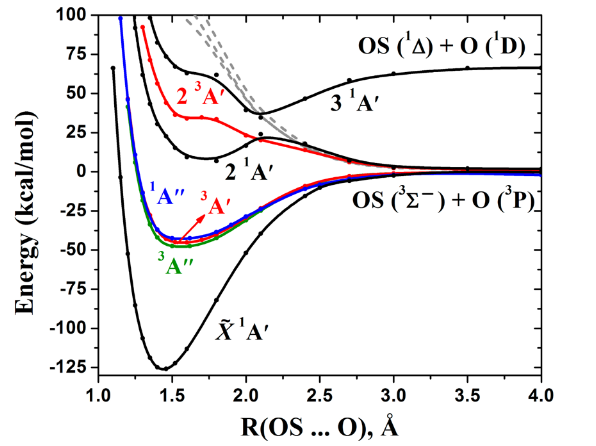

Figure 2. PECs of OSO as a function of the OS···O distance. The repulsive curves indicated by the dashed lines correspond to the quintet states.

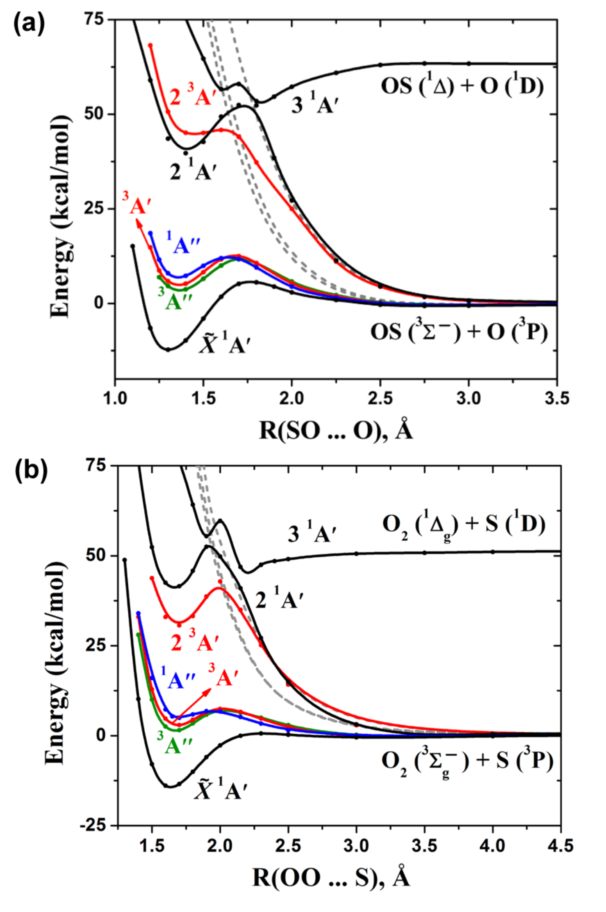

Figure 3. PECs of OOS as a function of (a) the SO···O and (b) the OO···S distances. The repulsive curves indicated by the dashed lines correspond to the quintet states.

variation of the biradical character within the XOX series, X = O, S, Se, Te, Po, and we observed that the electronegativity of the end atom X affects the magnitude of the biradical character: the less electronegative X is, the larger β becomes. The reason is the "increasing isolation" of the single electrons located on the end atoms X. In agreement with this picture, the biradical character increases from 0.180 for OOO to 0.260 for SOO and to 0.353 for SOS. However, when the central O atom is replaced by the less electronegative S atom, the biradical character of OSO decreases

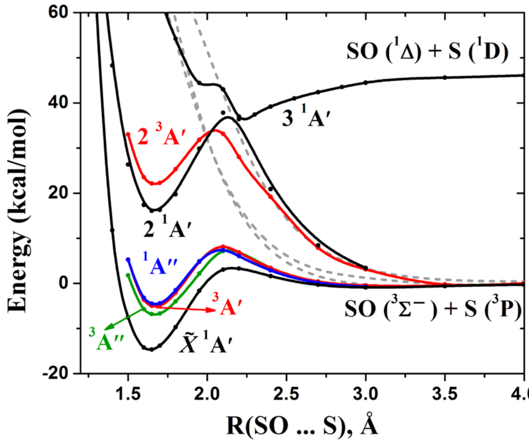

Figure 4. PECs of SOS as a function of the SO⋯S distance. The repulsive curves indicated by the dashed lines correspond to the quintet states.

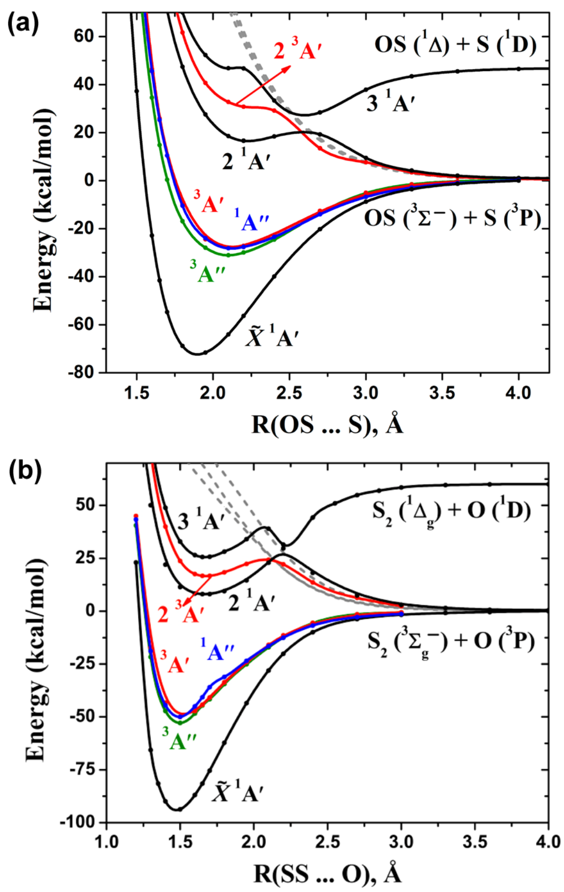

Figure 5. PECs of OSS as a function of (a) the OS⋯S and (b) the SS⋯O distances. The repulsive curves indicated by the dashed lines correspond to the quintet states.

to 0.035 (compared to 0.180 for OOO). Likewise, by replacing the central O atom with S, we obtain β = 0.044 for SSO and β = 0.108 and SSS, values that are much smaller than those for SOO (β = 0.260) and SOS (β = 0.353).

An interesting observation is that between the two SO_2 isomers the symmetric OSO structure is lower than the asymmetric SOO one by 114.9 kcal/mol, as opposed to OS_2 where the asymmetric SSO isomer is more stable than the symmetric SOS one by 58.7 kcal/mol. Recently, Dunning and

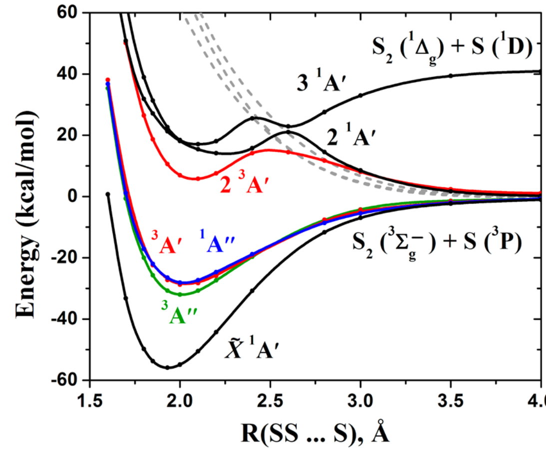

Figure 6. PECs of S_3 as a function of the SS⋯S distance. The repulsive curves indicated by the dashed lines correspond to the quintet states.

co-workers[24] reported results for the OSO and SOO isomers by applying the recoupled pair bond methodology. In particular, they considered the differences for the approach an O atom to either the S or the O end of the SO molecule. They observed that S is more eager to decouple its electron pairs and recouple them with the incoming oxygen electrons, explaining in this way the greater stability of OSO when compared to the SOO isomer and the larger biradical character of SOO when compared to OSO; these results are in complete agreement with the findings based on our present analysis.

Note that the PECs correlated to the ground-state fragments in Figures 2−5 follow the same pattern with the ground $\tilde{X}^1$ A′ state being well separated from the first three excited states (^{3}A″, ^{3}A′, ^{1}A″), which lie energetically very close to each other. In addition, the higher lying 2 ^{1}A′ and 2 ^{3}A′ and all three quintet states are in principle repulsive. The former two states, however, at shorter distances cross with higher excited states, and as a result they exhibit local minima.

In contrast to O_3, where the nearly degenerate ^{3}A″, ^{3}A′, and ^{1}A″ states bear nearly no barrier to the lowest asymptote, the minima of those states for its sulfur analogues do exhibit barriers to the lowest asymptote therefore being stable and in some cases (O−S−O, S−O−S, O−S−S, S_3) lie below the adiabatic fragments. More specifically, energy barriers are found whenever an oxygen or sulfur atom approaches the oxygen end of either the O_2 or the SO fragments. In contrast, the approach of the O or S atoms to the S terminal of S_2 or SO is barrierless. This observation indicates that the transition from the electronic picture of Scheme 7 (with 1.5 e^- to p_x and 1.5 e^- to p_y for each atom, see above) to the more appropriate picture for the bonding structures of Schemes 4−6 (with one e^- to p_x and two e^- to p_y or vice versa) is harder for the oxygen atom and easier for the larger sulfur atom. This behavior is consistent with the fact that sulfur produces polymers (S_4 up to S_{20} allotropic forms)[25] much easier than oxygen.[26]

The equilibrium wave functions of the first four states of all species are very similar to those described by eqs 5−8, albeit with a different numbering of the molecular orbitals and slightly different coefficients for the three excited states. Those different coefficients for the $\tilde{X}^1$ A′ states (cf. Table 1) affect the biradical character of the titled molecules and consequently their properties.

The wave function of the ground $\tilde{X}^1$ A′ state at infinity is identical for all species, and it is similar to the one in eq 9 with the appropriate change in the numbering of the molecular orbitals. The appearance of the four terms signaling the interaction with the $^1\Delta_{(g)}$ + ^{1}D fragments (see Section 3.1) occurs at different distances. Recall that in the O⋯OO PEC this happens at ~3.5 Å. The same distance is also observed in the O⋯OS PEC. For the four O⋯S cases (OS⋯O, OO⋯S, SO⋯S, O⋯SS) it takes place in the range from 4.0 to 4.25 Å, while for OS⋯S and SS⋯S at a distance of about 5.0 Å.

For the SSO and OSO isomers, which have the smallest biradical character (cf. Table 1), the MRCI wave function of the second ^{1}A′ state at its equilibrium distance (~1.8 Å) is

$$|2^1A'\rangle_{sso} \approx 0.48|7a'^2 1a''^2(2a''\overline{3a''} - \overline{2a''}3a'')\rangle - 0.44|7a'^2 1a''^2 2a''^2\rangle \quad (10)$$

$$|2^1A'\rangle_{oso} \approx 0.51|7a'^2 1a''^2(2a''\overline{3a''} - \overline{2a''}3a'')\rangle - 0.41|7a'^2 1a''^2 2a''^2\rangle \quad (11)$$

The first "ket" is the corresponding open singlet counterpart of the ^{3}A′ state (eq 6) arising from the ground state fragments, OS (X $^3\Sigma^-$) + O or S (^{3}P), while the second "ket" is the dominant component of the $\tilde{X}\,^1$A′ state arising from OS (X $^1\Delta$) + O or S (^{1}D). This is one more indication of the strong interaction between the two aforementioned channels. For the rest of the molecules, the first ket of eqs 10 and 11 appears in the repulsive 3^1A′ state.

4. CORRELATION BETWEEN THE BIRADICAL CHARACTER AND MOLECULAR PROPERTIES

The different mixing portions of the two bonding scenarios of Scheme 8 (see also Table 1) are expected to affect the geometrical and energetic properties (listed in Table 2) of the molecules under consideration. In this section we investigate the relation between the biradical character and those properties as well as the topology of the respective PECs of the species considered in this study. The questions we attempt to address are what those patterns are due to and whether they correlate with the molecular properties (and which ones) of the species or their fragments.

4.1. Bond Lengths. According to eq 6 and Scheme 4, the bonding in the ^{3}A′ state is mainly represented by the second scenario of Scheme 8 (electrons localized on the end atoms). As a result, large values of β for the ground $\tilde{X}\,^1$A′ indicate close similarity between the ^{1,3}A′ states. Indeed, their energy difference (T_e) is decreasing with increasing β with the exception when going from S_3 to O_3: T_e (β) [species] = 81.2 (0.035) [OSO], 44.2 (0.044) [SSO], 26.9 (0.108) [S_3], 30.8 (0.180) [O_3], 17.1 (0.260) [SOO], 9.6 (0.353) [SOS] kcal/mol. To the order of increasing β we plot the difference between the bond lengths of the ^{1,3}A′ states $\Delta r = r(^3A') - r(^1A')$ in Figure 7 (upper panel). In the case of the asymmetric isomers we used the average of the differences of the two nonequivalent bonds. The solid line in the upper panel of Figure 7 traces the line $\Delta r = -0.29048 \cdot \beta + 0.1316$ which best fits the data (r^2 = 0.9869).

From Table 2 it is also evident that the bond lengths of the ^{1}A″ and ^{3}A″ states are very similar (differing no more than 0.007 Å) with the exception of the SO and SS bonds of SOO and SSO, which differ by 0.016 and 0.025 Å, respectively. This observation is consistent with the fact that both states can be described by the bonding scenario shown in Scheme 4.

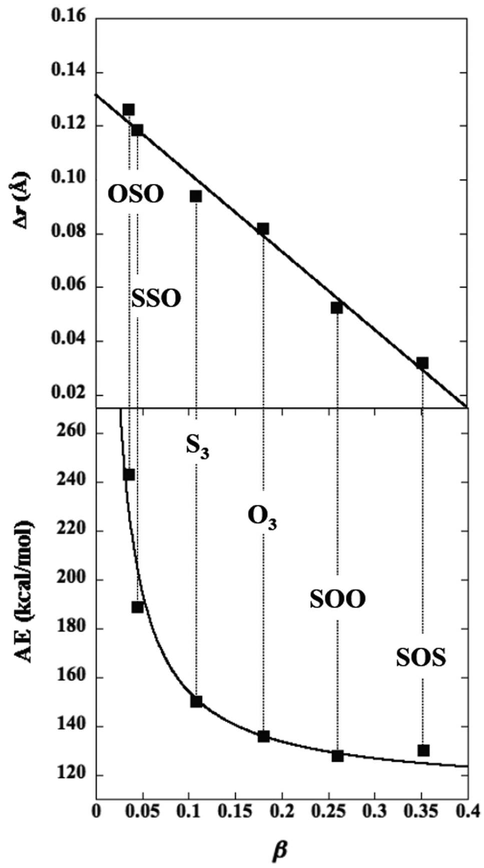

Figure 7. Differences between the bond lengths (Δr) of the $\tilde{X}^1$ A′ and ^{3}A′ states (upper panel) and atomization energies (AEs) of the $\tilde{X}^1$ A′ states (lower panel) for all studied species as a function of the biradical character (β). For the asymmetric species (OSS, OOS) the average of the two differences for the distances is used. Lines trace least-mean squares fits to the data (see text).

We subsequently examine the change in the OO, SS, and SO bond lengths among the several species. The two OO distances are 1.279 Å (O_3) and 1.308 Å (OOS), while the two SS distances are 1.934 Å (S_3) and 1.897 Å (SSO). In both cases, the larger biradical character corresponds to longer bonds, as expected due to Scheme 8. Similarly, the four different SO lengths with the corresponding β values are 1.438 Å (in OSO, β = 0.035), 1.475 Å (in SSO, β = 0.044), 1.639 Å (in SOO, β = 0.260), and 1.640 Å (in SOS, β = 0.353) following the same trend.

4.2. Atomization Energies. The AE, viz. the energy needed to fully dissociate the titled molecules to the O(^{3}P) and/or S(^{3}P) atoms, are given in Table 1. As shown in Figure 7 (lower panel) the AEs vary as ~$1/\beta$, i.e., larger AEs are associated with molecules with smaller biradical character and vice versa. The reason is that, according to the discussion related to Scheme 8, a large β results in a smaller bond order (i.e., a "weaker" covalent bond) and consequently for a smaller AE as the minimum is further destabilized with respect to the atomic fragments. The solid line in the lower panel of Figure 7 corresponds to the function AE = 112.97 + 4.0993/β, which best fits the data (r^2 = 0.94783).

An immediate consequence of the increasing AE with decreasing β is that for SO_2 the symmetric isomer is lower in energy than the asymmetric one, but the opposite is true for OS_2 (asymmetric isomer is lower in energy). Both isomers of SO_2 (OSO/OOS) and OS_2 (OSS/SOS) correlate with the same atomic fragments, viz. $S(^3P) + 2O(^3P)$ and $O(^3P) + 2S(^3P)$, however the (symmetric) OSO and (asymmetric) OSS isomers have a smaller biradical character than the (asymmetric) OOS and (symmetric) SOS and therefore larger AEs.

4.3. The XY−Z Bond Energy. The PECs shown in Figures 1−6 identify several trends. Figure 8 collects the information

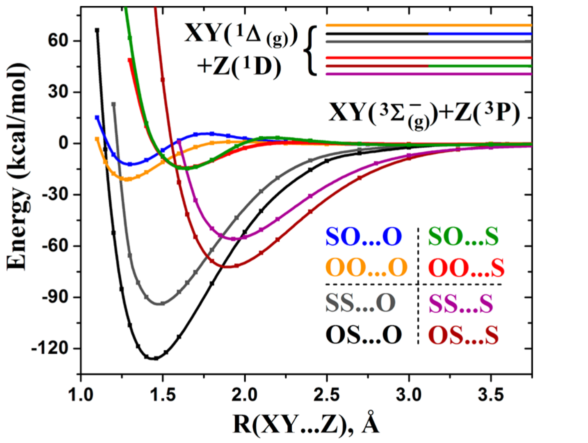

Figure 8. Summary of the ground-state PECs from Figures 1−6. Horizontal solid lines denote the excited states of the asymptotic fragments XY ($^1\Delta_{(g)}$) + Z (^{1}D). Note the grouping per pair according to the bond that is being broken along the PEC.

of the ground-state PECs for the XYZ molecules along the XY⋯Z distance with respect to the lowest XY ($^3\Sigma^-_{(g)}$) + Z (^{3}P) asymptote. The horizontal solid lines in the upper right corner of Figure 8 are color coded to indicate the corresponding XY ($^1\Delta_{(g)}$) + Z (^{1}D) asymptotes, viz. the energy levels matching the sum of the first excited states of the XY and Z fragments. It is readily seen that the 8 ground-state PECs of Figures 1−6 fall into 4 different groups of pairs (demarcated by the dotted lines in the lower right of Figure 8) according to the Y−Z bond that is being broken and the nature of the Y atom. The 4 pairs of PECs are therefore: (1) SO⋯O/OO⋯O, (2) SO⋯S/OO⋯S, (3) SS⋯O/OS⋯O, and (4) SS⋯S/OS⋯S. Each pair has XY−Z bond energies of similar magnitude as well as nearly identical XY⋯Z distances at the corresponding global minima. The bond energies range from 11.6 to 126.5 kcal/mol (see Table 1). As noted in the previous section, the first two groups of pairs (SO⋯O/OO⋯O and SO⋯S/OO⋯S) also have small barriers with respect to the lowest asymptote, whereas the last two (SS⋯O/OS⋯O and SS⋯S/OS⋯S) do not. In the following we will investigate the correlation between the ground-state XY−Z bond energies and the position of the excited states of the XY and Y fragments through the biradical character of the XYZ minimum.

Pursuing the schematic drawing and definitions of Figure 9:

$$E_B = E_T - (T_1 + T_2) \tag{12}$$

where E_B is the XY−Z bond energy, E_T the energy difference between the XYZ minimum and the energy level corresponding to the sum of the excited states of the XY and Z fragments, viz. XY ($^1\Delta_{(g)}$) + Z (^{1}D), and T_1, T_2 denote the excitation energies of the XY and Z fragments, i.e., $T_1 = E(^1\Delta_{(g)}) - E(^3\Sigma^-_{(g)})$ of XY and $T_2 = E(^1D) - E(^3P)$ of Z. The higher the excited states of the XY and Z fragments are, the smaller their interaction (and subsequent mixing) with the ground-state asymptote is and consequently the smaller the biradical character of XYZ,

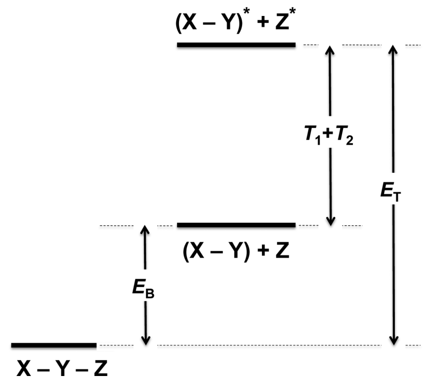

Figure 9. Energy diagram showing the bond energy (E_B) of (XY−Z), the excitation energies (T_1, T_2) of fragments (X−Y) and Z and the energy difference between the ground state (X−Y−Z) and the excited XY ($^1\Delta_{(g)}$) + Z (^{1}D) fragments (E_T).

suggesting that $E_T \sim 1/\beta$. This trend is consistent with the variation of the AEs with $1/\beta$ discussed in the previous section.

A regression analysis of the multiple linear model:

$$E_B = A\cdot\left(\frac{1}{\beta}\right) + B\cdot T_1 + C\cdot T_2 + D \tag{13}$$

for the dependent variable E_B with respect to the three independent variables $1/\beta$, T_1 and T_2 with 8 data points (O_3, OSO, OSS (2), OOS (2), SOS and S_3) yielded $A = 3.7595$, $B = -1.48775$, $C = 0.199754$, and $D = 24.0988$ with a correlation coefficient $r^2 = 0.9483$. The correlation between the calculated XY−Z bond energies (listed in Table 1) and the ones predicted from the model (eq 13) is shown in Figure 10. Overall the

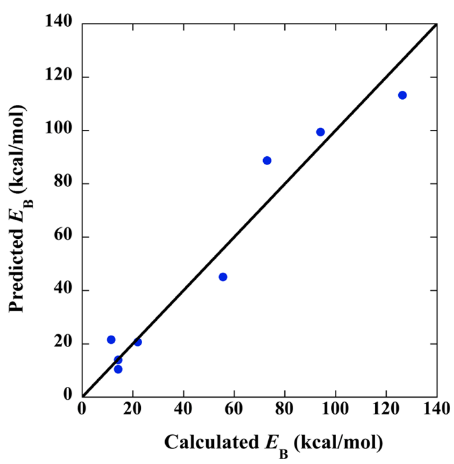

Figure 10. Calculated (X−YZ)/(XY−Z) bond energies (E_B) (cf. Table 1) versus the ones predicted from eq 13.

assumed model, eq 13, was found to predict the calculated bond energies quite satisfactorily. Therefore the different strengths of the XY−Z bonds can be related to the biradical character of the XYZ species and the excitation energies of the lowest asymptotic fragments.

The fact that larger XY−Z bond energies are associated with molecules with smaller β can furthermore account for the morphology of the ground-state PECs depicted in Figures 1−6 and summarized in Figure 8: PECs that describe molecules having large β (SO⋯O, OO⋯O, SO⋯S, and OO⋯S) have small barriers with respect to the lowest asymptote, whereas the ones

dx.doi.org/10.1021/ja410726u | J. Am. Chem. Soc. 2014, 136, 2808−2817

describing molecules with small β (SS···O, OS···O, SS···S and OS···S) do not. This is because the smaller the β, the larger the XY−Z bond energy is, and therefore the more stable the equilibrium structure (see also Section 4.1). It is the stabilization of the equilibrium structure that pushes the whole PEC to lower energies thus eliminating the barrier (French curve effect).

5. CONCLUSIONS

The analysis of the ground-state MRCI wave function at the minimum energy geometries allows for the definition of a simple quantity, the biradical character β, which measures the relative mixture of different bonding scenarios in the triatomic X−Y−Z molecules, where X, Y, Z = O, S. For these systems, the first picture (with weight $1-\beta$) corresponds to a closed-shell wave function with a single σ bond between the central and the end atoms and one π bond shared among the three atoms, whereas the second picture (with weight β) can be derived from the first one by decoupling the two π-bonded electrons and localizing them on the end atoms. The magnitude of β ranges from 0 (a pure closed shell, i.e. a 100 to 0% mixture) to 1 (a perfect biradical, i.e., a 0 to 100% mixture between the two bonding scenarios). In this respect, our analysis provides a quantitative measure of the mixing between the classical Lewis structures that can be used to represent the bonding in those systems. Ozone was found to have a 82−18 mixture of the two bonding pictures (β = 0.180), a result that lies between the two extreme views proposed earlier.[6,7] The biradical character of ozone's sulfur analogues is listed in Table 3 along with the corresponding percentages of the two bonding scenarios, with the O−S−O (β = 0.035) and S−O−S (β = 0.353) molecules being the two extremes of the series. In essence, the electronegativity of the end atoms compared to the central one is the prevailing factor for determining the magnitude of β as the two extreme values in the series are suggesting.

Table 3. Proposed Bonding Pattern and Corresponding Bond order for the X−Y−Z Triatomics, where X, Y, Z = O, S

Molecule (X–Y–Z)	Biradical character (β)	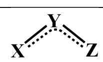 $(1-\beta)$	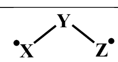 (β)	Bond Order $(3-\beta)/2$
O–S–O	0.035	96.5 %	3.5 %	1.483
O–S–S	0.044	95.6 %	4.4 %	1.478
S–S–S	0.108	89.2 %	10.8 %	1.446
O–O–O	0.180	82.0 %	18.0 %	1.410
O–O–S	0.260	74.0 %	26.0 %	1.370
S–O–S	0.353	64.7 %	35.3 %	1.324

Furthermore, the suggested analysis naturally allows for the definition of a bond order, which is equal to $(3-\beta)/2$, for the covalent bonds in these systems that varies from 1.5 (for a pure closed shell, $\beta = 0$) to 1 (for a perfect biradical, $\beta = 1$). The corresponding bond orders for all six molecules studies here are also listed in Table 3. Our analysis explains the different O−O, S−S, or S−O bond lengths in the molecules under consideration. These bond orders are directly related to the energetic stabilization of the corresponding minima with respect to the O(^{3}P) and/or S(^{3}P) atomic fragments since larger bond orders (smaller β) are associated with covalent bonds that are harder to "break"; indeed the atomization energies (AEs) for the series were found to vary as $1/\beta$. This can further account for the relative stability of the different isomers corresponding to symmetric and asymmetric structures, viz. OSS/SOS and OOS/OSO via the realization of their different biradical characters.

In general, larger β values (i.e., cases where there is a larger percentage of the second picture in the mixture), result in a smaller energy gap and more similar geometries between the ground ^{1}A′ and first excited ^{3}A′ states, the larger atomization and XY−Z binding energies of the ground-state minima and the gradual elimination of barriers at the ground-state PEC from equilibrium to the lowest energy asymptotic fragments. In this respect the notion of the biradical character provides, via the analysis of the electronic structure, a quantitative tool that can account for several trends in the structural and energetic properties of the series comprising of ozone and its sulfur analogues.

■ AUTHOR INFORMATION

Corresponding Author

sotiris.xantheas@pnnl.gov

Notes

The authors declare no competing financial interest.

■ ACKNOWLEDGMENTS

This work was supported by the U.S. Department of Energy, Office of Basic Energy Sciences, Division of Chemical Sciences, Geosciences and Biosciences. Pacific Northwest National Laboratory (PNNL) is a multiprogram national laboratory operated for DOE by Battelle. This research used resources of the National Energy Research Scientific Computing Center, which is supported by the Office of Science of the U.S. Department of Energy under contract no. DE-AC02-05CH11231.

■ REFERENCES

(1) (a) Bermúdez-Aguirre, D.; Barbosa-Cánovas, G. V. *Food Control* **2012**, *29*, 82−90. (b) Miller, F. A.; Silva, C. L. M.; Brandão, T. R. S. *Food Eng. Rev.* **2013**, *5*, 77−106.

(2) (a) Lee, H.; Lee, E.; Lee, C.-H.; Lee, K. *J. Ind. Eng. Chem.* **2011**, *17*, 468−473. (b) Penru, Y.; Guastalli, A. R.; Esplugas, S.; Baig, S. *Ozone: Sci. Eng.* **2013**, *35*, 63−70.

(3) Logan, J. A. *J. Geophys. Res.* **1985**, *90*, 10463−10482.

(4) Andersen, S. O.; Halberstadt, M. L.; Borgford-Parnell, N. *J. Air Waste Manage. Assoc.* **2013**, *63*, 607−647.

(5) (a) Rubin, M. B. *Helv. Chim. Acta* **2003**, *86*, 930−939. (b) Bailey, P. S. *Chem. Rev.* **1958**, *58*, 925−1010. (c) Griffith, W. P. *Coord. Chem. Rev.* **2001**, *219*−*221*, 259−281. (d) Van Ornum, S. G.; Champeau, R. M.; Pariza, R. *Chem. Rev.* **2006**, *106*, 2990−3001.

(6) Hay, P. J.; Dunning, T. H., Jr.; Goddard, W. A. *J. Chem. Phys.* **1975**, *62*, 3912−3924.

(7) Kalemos, A.; Mavridis, A. *J. Chem. Phys.* **2008**, *129*, 054312.

(8) Miliordos, E.; Ruedenberg, K.; Xantheas, S. S. *Angew. Chem., Int. Ed.* **2013**, *52*, 5736−5739.

(9) (a) Hayes, E. F.; Siu, A. K. Q. *J. Am. Chem. Soc.* **1971**, *93*, 2090−2091. (b) Laidig, W. D.; Schaefer, H. F., III *J. Chem. Phys.* **1981**, *74*, 3411−3414. (c) Schmidt, M. W.; Gordon, M. S *Annu. Rev. Phys. Chem.* **1998**, *49*, 233−266. (d) Oyedepo, G. A.; Wilson, A. K. *J. Phys. Chem. A* **2010**, *114*, 8806−8816.

(10) Glezakou, V. A.; Elbert, S. T.; Xantheas, S. S.; Ruedenberg, K. *J. Phys. Chem. A* **2010**, *114*, 8923−8931.

(11) Xantheas, S. S.; Atchity, G. J.; Elbert, S. T.; Ruedenberg, K. *J. Chem. Phys.* **1991**, *94*, 8054.

(12) (a) Knowles, P.; Werner, H.-J. *Chem. Phys. Lett.* **1988**, *145*, 514. (b) Werner, H.-J.; Knowles, P. *J. Chem. Phys.* **1988**, *89*, 5803.

(13) Werner, H.-J.; Knowles, P. J.; Knizia, G.; Manby, F. R.; M. Schütz, Celani, P.; Korona, T.; Lindh, R.; Mitrushenkov, A.; Rauhut, G.; Shamasundar, K. R.; Adler, T. B.; Amos, R. D.; Bernhardsson, A.; Berning, A.; Cooper, D. L.; Deegan, M. J. O.; Dobbyn, A. J.; Eckert, F.; Goll, E.; Hampel, C.; Hesselmann, A.; Hetzer, G.; Hrenar, T.; Jansen, G.;

C. Köppl, Liu, Y.; Lloyd, A. W.; Mata, R. A.; May, A. J.; McNicholas, S. J.; Meyer, W.; Mura, M. E.; Nicklass, A.; D. P. O'Neill, Palmieri, P.; Peng, D.; K. Pflüger, Pitzer, R.; Reiher, M.; Shiozaki, T.; Stoll, H.; Stone, A. J.; Tarroni, R.; Thorsteinsson, T.; Wang, M. *MOLPRO, version 2012.1, a package of ab initio programs*; University College Cardiff Consultants, Ltd.: Cardiff, U.K., 2012; http://www.molpro.net.

(14) (a) Dunning, T. H., Jr. *J. Chem. Phys.* **1989**, *90*, 1007. (b) Kendall, R. A.; Dunning, T. H., Jr.; Harrison, R. J. *J. Chem. Phys.* **1992**, *96*, 6796.

(15) Dunning, T. H., Jr.; Peterson, K. A.; Wilson, A. K. *J. Chem. Phys.* **2001**, *114*, 9244−9253.

(16) Pilar, F. L., *Elementary Quantum Chemistry*; McGraw-Hill Book Company: New York, 1968.

(17) (a) Huber, K.; Herzberg, G. H. *Molecular Spectra and Molecular Structure. In Constants of Diatomic Molecules*; Van Nostrand Reinhold: New York, 1979; Vol. *IV*; (b) Kramida, A.; Ralchenko, Y.; Reader, J., and NIST ASD Team. *NIST Atomic Spectra Database*, version 5.0, online; National Institute of Standards and Technology: Gaithersburg, MD, 2012; http://physics.nist.gov/asd (accessed July 3, 2013).

(18) (a) Banichevich, A.; Pyerimhoff, S. D.; Grein, F. *Chem. Phys. Lett.* **1990**, *173*, 1−6. (b) Banichevich, A.; Pyerimhoff, S. D.; Grein, F. *Chem. Phys. Lett.* **1992**, *195*, 459−468. (c) Banichevich, A.; Pyerimhoff, S. D.; Grein, F. *Chem. Phys.* **1993**, *178*, 155−188.

(19) (a) Grebenshchikov, S. Y.; Qu, Z.-W.; Zhu, H.; Schinke, R. *Phys. Chem. Chem. Phys.* **2007**, *9*, 2044−2064. (b) Schinke, R.; McBane, G. C. *J. Chem. Phys.* **2010**, *132*, 044305.

(20) (a) Muller, T.; Xantheas, S. S.; Dachsel, H.; Harrison, R. J.; Nieplocha, J.; Shepard, R.; Kedziora, G.; Lischka, H. *Chem. Phys. Lett.* **1998**, *293*, 72. (b) Han, H.; Suo, B.; Xie, D.; Lei, Y.; Wang, Y.; Wen, Z. *Phys. Chem. Chem. Phys.* **2011**, *13*, 2723−2731. (c) Hino, O.; Kinoshita, T.; Chan, G. K.-L.; Bartlett, R. J. *J. Chem. Phys.* **2006**, *124*, 114311.

(21) (a) Xantheas, S. S.; Elbert, S. T.; Ruedenberg, K. *J. Chem. Phys.* **1990**, *93*, 7519. (b) Atchity, G. J.; Xantheas, S. S.; Ruedenberg, K. *J. Chem. Phys.* **1991**, *95*, 1862. (c) Atchity, G. J.; Ruedenberg, K. *J. Chem. Phys.* **1993**, *99*, 3790. (d) Ivanic, J.; Atchity, G. J.; Ruedenberg, K. *J. Chem. Phys.* **1997**, *107*, 4307.

(22) Peterson, K. A.; Lyons, J. R.; Francisco, J. S. *J. Chem. Phys.* **2006**, *125*, 084314.

(23) (a) Becker, S.; Braatz, C.; Lindner, J.; Tiemann, E. *Chem. Phys.* **1995**, *196*, 275−291. (b) Chen, L.-S.; Lee, C. I.; Lee, Y. P. *J. Chem. Phys.* **1996**, *105*, 9454−9460. (c) Du, S.; Germann, T. C.; Francisco, J. S.; Peterson, K. A.; Yu, H.-G.; Lyons, J. R. *J. Chem. Phys.* **2011**, *134*, 154508. (d) Elliott, R.; Compton, R.; Levis, R.; Matsika, S. *J. Phys. Chem. A* **2005**, *109*, 11304−11311. (e) Francisco, J. S.; Lyons, J. R.; Williams, I. H. *J. Chem. Phys.* **2005**, *123*, 054302. (f) Han, H.; Suo, B.; Jiang, Z.; Wang, Y.; Wen, Z. *J. Chem. Phys.* **2008**, *128*, 184312. (g) Ivanic, J.; Atchity, G. J.; Ruedenberg, K. *J. Chem. Phys.* **1997**, *107*, 4307−4317. (h) Lévêque, C.; Komainda, A.; Taïeb, R.; Köppel, H. *J. Chem. Phys.* **2013**, *138*, 044320. (i) Li, A.; Suo, B.; Wen, Z.; Wang, Y. *Sci. China, Ser. B: Chem.* **2006**, *49*, 289−295. (j) McCarthy, M. C.; Thorwirth, S.; Gottlieb, C. A.; Thaddeus, P. *J. Am. Chem. Soc.* **2004**, *126*, 4096−4097. (k) Nachtigall, P.; Hrušák, J.; Bludský, O.; Iwata, S. *Chem. Phys. Lett.* **1999**, *303*, 441−446. (l) Thorwirth, S.; McCarthy, M. C.; Gottlieb, C. A.; Thaddeus, P.; Gupta, H.; Stanton, J. F. *J. Chem. Phys.* **2005**, *123*, 054326. (m) Ulenikov, O. N.; Bekhtereva, E. S.; Alanko, S.; Horneman, V.-M.; Gromova, O. V.; Leroy, C. *J. Mol. Spectrosc.* **2009**, *257*, 137−156. (n) Zhang, Y. F.; Wang, M. S.; Ma, M. Z.; Ma, R. C. *J. Mol. Structure: THEOCHEM* **2008**, *859*, 7−10. (o) Lo, W.-J.; Wu, Y.-J.; Lee, Y.-P. *J. Chem. Phys.* **2002**, *117*, 6655−6661. (p) Lo, W.-J.; Wu, Y.-J.; Lee, Y. P. *J. Phys. Chem. A* **2003**, *107*, 6944−6947.

(24) Lindquist, B. A.; Takeshita, T. Y.; Woon, D. E.; Dunning, T. H. J. *J. Chem. Theory Comput.* **2013**, *9*, 4444.

(25) Greenwood, N. N.; Earnshaw, A. *Chemistry of the Elements*, 2nd ed.; Elsevier Ltd: Oxford, 1997, pp 652−661.

(26) Gadzhiev, O. B.; Ignatov, S. K.; Kulikov, M. Y.; Feigin, A. M.; Razuvaev, A. G.; Sennikov, P. G.; Schrems, O. *J. Chem. Theory Comput.* **2013**, *9*, 247−262.

(27) Chase, M. W., Jr.; Davies, C. A.; Downey, J. R., Jr.; Frurip, D. J.; McDonald, R. A.; Syverud, A. N. *J. Phys. Chem. Ref. Data* **1985**, *14*, 1.

(28) Jones, A. V. *J. Chem. Phys.* **1950**, *18*, 1263−1268.

(29) Tyuterev, V. G.; Tashkun, S.; Jensen, P.; Barbe, A.; Cours, T. *J. Mol. Spectrosc.* **1999**, *198*, 57−76.

(30) Bouvier, A. J.; Inard, D.; Veyret, V.; Bussery, B.; Bacis, R.; Churassy, S.; Brion, J.; Malicet, J.; Judge, R. H. *J. Mol. Spectrosc.* **1998**, *190*, 189−197.

(31) Grünther, J.; Anderson, S. M.; Hilpert, G.; Mauersberger, K. *J. Chem. Phys.* **1998**, *108*, 5449−5457.

(32) Arnold, W.; Xu, C.; Kim, E. H.; Neumark, D. M. *J. Chem. Phys.* **1994**, *101*, 912−922.

(33) (a) Morino, Y.; Kikuchi, Y.; Saito, S.; Hirota, E. *J. Mol. Spectrosc.* **1964**, *13*, 95−118. (b) Saito, S. *J. Mol. Spectrosc.* **1969**, *30*, 1−16.

(34) Lindenmayer, J.; Rudolph, H. D.; Jones, H. *J. Mol. Spectrosc.* **1986**, *119*, 56−67.

(35) Tsukiyama, K.; Kobayashi, D.; Obi, K.; Tanaka, I. *Chem. Phys.* **1984**, *84*, 337−343.